UNSATURATED PARTICULATE MATERIALS—PARTICLE-LEVEL STUDIES

By Gye Chun Cho[1] and J. Carlos Santamarina,[2] Member, ASCE

ABSTRACT: Analyses and experiments are performed to gain further insight into the behavior of unsaturated particulate materials, with emphasis on the pendular stage. First, interparticle forces are computed based on Laplace's equation; soil particles are ideally considered spherical or flat to facilitate the identification of the most relevant factors that affect unsaturated soil behavior. Second, the small strain stiffness is continuously measured on specimens subjected to drying, and changes in stiffness are related to changes in interparticle forces; data show important differences with previously published trends based on remolded specimens. Third, microscale experiments are performed to assess the strain at menisci failure in multiple deformation modes; results indicate that the lower the water content, the lower the strain required to eliminate the effects of capillarity, therefore, while capillary forces affect small strain stiffness, they may not contribute to large strain stiffness or strength. Finally, the rate of menisci regeneration is studied after a perturbation; stiffness recovery decreases with decreasing water content, and full recovery may not be reached when the degree of saturation is low. Several phenomena associated with the evolution of capillary forces during drying are identified.

INTRODUCTION

Soils are particulate materials, thus, their properties are governed by interparticle forces. In unsaturated soils, the negative pore-water pressure in menisci at particle contacts increases the interparticle forces, changes the small-strain stiffness, and alters the soil strength. Furthermore, all forms of conduction and diffusion processes depend on the size and connectivity of menisci. Such effects are not readily considered within the framework of classical soil mechanics.

The fundamental phenomena that are related to the behavior and effects of water in unsaturated particulate materials are reviewed first. Then, analyses and experiments are performed to gain further insight into the behavior of unsaturated particulate materials with emphasis on particle-level studies. These studies include microscale analysis of interparticle forces, assessment of small strain stiffness in relation to interparticle forces, and menisci failure during straining and subsequent recovery.

WATER IN UNSATURATED SOILS—EFFECTIVE STRESS

Fundamental Concepts and Relations

The behavior of water in unsaturated particulate materials is related to phenomena such as vapor pressure, evaporation, suction, and cavitation. Molecules at the gas-liquid interface tend to leave the liquid due to thermal agitation. The number of molecules in the vapor phase increases, until the number of molecules returning to and leaving the liquid is balanced. At this point, the vapor is said to be saturated, and its pressure is called the saturated vapor pressure (Giancoli 1998). Clearly, the saturated vapor pressure depends on temperature. That is, the higher the temperature, the higher the kinetic energy that molecules have to break away from the liquid into the vapor phase. Hence, the pressure at which equilibrium is reached increases with temperature (the vapor pressure at temperature 100°C is 100 kPa).

Water evaporation (or the rate of drying) depends mainly on heat supply, surrounding vapor pressure, and water availability/supply (Fisher 1923; Gilliland 1938; Oliver and Newitt 1949; Hillel 1980). In addition, soluble salts in the pore water cause a decrease in the rate of drying because the vapor pressure difference between the liquid and the air decreases (Kayyal 1995). The presence of salts adds an osmotic component to suction as well.

As water evaporates from saturated soils during drying, the air-water interface starts to curve due to pressure difference between the air and the water phase. The vapor pressure is affected by the curvature of the air-water interface as expressed in Kelvin's equation (Defay and Prigogine 1966)

$$\underline{R}T \ln \frac{P}{P_0} = -\frac{M}{\rho} T_s \left(\frac{1}{r_1} + \frac{1}{r_2}\right) \tag{1}$$

where r_1 and r_2 = two principal radii at the curved interface (Fig. 1); P_0 = normal vapor pressure at the free liquid; P = vapor pressure observed at the curved interface; T = absolute temperature; $\underline{R}$ = universal (molar) gas constant (i.e, 8.31 N·m/mol·K); $\overline{M}$ = molecular weight of the liquid; ρ = liquid density; and T_s = surface tension (i.e., 0.0727 N/m at 20°C).

The pressure difference Δu between the air pressure u_a and the water pressure u_w also depends on the curvature of the interface characterized by radii r_1 and r_2 and the surface tension T_s (Fig. 1). According to Laplace's equation

$$\Delta u = (u_a - u_w) = T_s \left(\frac{1}{r_1} + \frac{1}{r_2}\right) \tag{2}$$

The pressure difference $\Delta u = (u_a - u_w)$ is often referred to as matric suction. Since the pore air pressure, in general, is greater than the pore-water pressure, the matric suction has a positive value. If the air pressure u_a is considered as a reference (e.g., the atmospheric pressure), the pore-water pressure is negative and its absolute value is the same as the right-hand side in (2). In the presence of soluble salts, the total suction (or soil suction) consists of matric suction and osmotic suction.

The rupture of the liquid or cavitation may take place when suction increases. The cavitation pressure depends on the tensile strength of the liquid. In large volumes (i.e., saturated condition), water at 20°C cavitates when the water pressure reaches $u_w \approx -100$ kPa. However, water can sustain high tension under appropriate conditions. This fact has long been recognized in soil mechanics (Terzaghi 1925; Hilf 1956; Skempton 1961; Bishop et al. 1975; Fredlund 1991). The theoretical tensile strength of water is in the order of thousands of atmospheres (Fisher 1948; Guan and Fredlund 1997). Water under tension is in a metastable condition until nucleation occurs, i.e., the formation of vapor cavities within the liquid itself or at their boundaries (Trevena 1987). Therefore, cavi-

[1]Grad. Student, Civ. and Envir. Engrg., Georgia Inst. of Technol., Atlanta, GA 30332.

[2]Prof., Civ. and Envir. Engrg., Georgia Inst. of Technol., Atlanta, GA. E-mail: carlos@ce.gatech.edu

Note. Discussion open until June 1, 2001. To extend the closing date one month, a written request must be filed with the ASCE Manager of Journals. The manuscript for this paper was submitted for review and possible publication on February 17, 1999. This paper is part of the ***Journal of Geotechnical and Geoenvironmental Engineering***, Vol. 127, No. 1, January, 2001. ©ASCE, ISSN 1090-0241/01/0001-0084–0096/$8.00 + $.50 per page. Paper No. 20207.

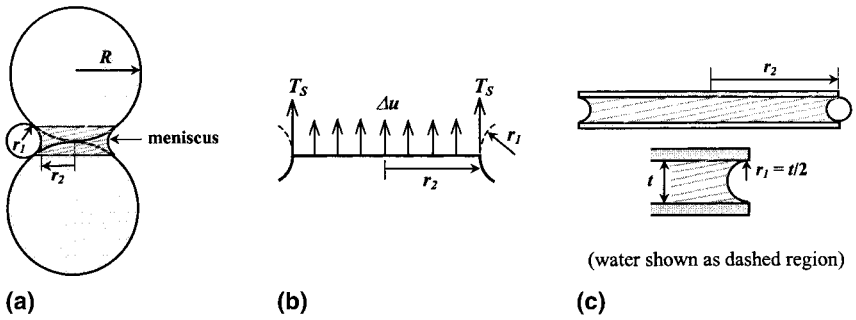

FIG. 1. Microscale Models—Schematic Representation: (a) Spherical Particles; (b) Forces Involved; (c) Disk Particles

tation is hindered in the absence of cavitation nuclei and experimental values as low as −17 MPa (−170 atm) have been obtained (Marinho and Chandler 1995).

Stages of Saturation

Different stages of saturation can be identified. As water begins evaporating or draining from a saturated soil, the outside menisci at boundaries are pulled inward and the suction pressure increases [as predicted by (2)]. While the change in water content is very small, the change in pore-water pressure has an important global effect on the soil mass which remains saturated away from the boundary.

The pressure when the air phase breaks through into the pore structure is called the air-entry value (also known as bubbling pressure or threshold pressure) (Bear 1979; Kohgo et al. 1993; Aubertin et al. 1998). The air-entry value depends on the pore size, thus, the finer the particles the smaller the pore throats and the higher the air-entry value. Air entry generally occurs between saturation $S = 0.9$ and $S = 1.0$.

Once air breaks in, the soil mass becomes unsaturated, yet, the water still forms a continuous phase. This is the funicular stage (Newitt and Conway-Jones 1958; Pietsch 1991; Leverson and Lohnes 1995). As drying proceeds, the suction pressure increases gradually, following a quasi-linear trend with decreasing saturation. Any local change in water pressure is rapidly homogenized throughout the mass by pressure diffusion within the continuous water phase. The drying rate is rather constant in this region.

The pendular stage begins when water becomes disconnected. Water rings form around particle contacts, and only an adsorbed film may be present on particle surfaces (Leverson and Lohnes 1995). The radii of menisci are small, thus the suction pressure increases significantly. Because this is only a contact-level effect, a change in suction within a meniscus is felt at other menisci through the corresponding change in vapor pressure [(1)]. This is a slow homogenization process. The drying rate in this stage is increasingly lower.

Since an unsaturated soil implies a mixed fluid phase, two percolation thresholds can be identified according to the continuity of each phase. One threshold corresponds to the formation of a continuous gas phase path. This threshold separates regimes with very different coefficients of air permeability. The other percolation threshold S_c occurs when a continuous water film forms across the particulate medium, i.e., the boundary between the pendular and the funicular regimes. Electrical conduction and chemical diffusion in unsaturated media rapidly increase when the degree of saturation exceeds S_c. Both percolation thresholds are different during drying or wetting processes. Furthermore, given the fractal nature of the connectivity structure of a phase near percolation, measured parameters depend on specimen size (Sahimi 1994).

The matric suction can be measured with general tensiometers up to 1 atm, or through high air entry ceramics above 1 atm (cavitation within the measurement system is avoided by the axis-translation technique, as discussed in Fredlund and Rahardjo 1993). Additionally, from Kelvin's equation, total suction can be inferred from the vapor pressure, or measured with psychrometers, for example, in the pendular stage. However, as discussed above, salts affect the vapor pressure, thus psychrometers sense both the pore-water pressure (air pressure is presumed atmospheric) and the osmotic suction. Values of matric suction can vary from as low as 10^{-1} kPa in clean sands to more than 10^3 kPa in clays.

Effective Stress—Macroscale

Equilibrium analysis in saturated media leads to Terzaghi's effective stress

$$\sigma' = \sigma - u_w \tag{3}$$

Likewise, the negative pore-water pressure that develops in an unsaturated medium affects the effective interparticle forces. However, the equilibrium analysis must take into consideration the reduced area occupied by the water in the pores. Bishop (1959, 1961) proposed a modified expression for the effective stress in an unsaturated soil

$$\sigma' = (\sigma - u_a) + \chi(u_a - u_w) \tag{4}$$

where χ = parameter to be experimentally determined. To a first approximation, the parameter χ varies with the degree of saturation, from $\chi \approx 1$ for saturated soils, to $\chi = 0$ for dry soils (Aitchison and Donald 1956; Aitchison 1960; Blight 1967). However, χ also depends on wetting history, loading path, soil type, internal structure of the soil, and specimen size near percolation (as mentioned above). Still, the inadequacy in Bishop's equation goes beyond the difficulty in predicting the value of χ, and it can fail to explain phenomena such as the collapse of some soils upon wetting (u_w decrease σ' decreases, yet massive volume change takes place).

The limitations in Bishop's equation can be discussed from different perspectives. On the one hand, it involves a soil parameter χ as in a constitutive equation rather than being a description of the state of stress. On the other hand, it mixes global and local conditions. In Terzaghi's effective stress equation for saturated media, both pore pressure and total stress are boundary actions; however, the pore-water pressure in unsaturated soils causes a local action at the particle level (this is more readily seen in the pendular regime but it is the case in the funicular regime as well).

Today's macroscale interpretation of unsaturated materials is based on separate state variables, such as $(u_a - u_w)$ and $(\sigma - u_a)$ to avoid such limitations (Bishop and Blight 1963; Fredlund et al. 1978).

MICROSCALE ANALYSIS

The equivalent effective stress σ'_{eq}, due to capillarity is herein defined as the effective boundary stress that should be applied to a dry or saturated soil specimen to cause similar

interparticle contact forces. The following study starts with Laplace's relation [i.e., (2)] and leads to the prediction of the equivalent effective stress as a function of water content, and particle size or specific surface. The purpose of the microscale analyses is not to predict field parameters, but to highlight the interplay between the variables involved. Soil particles are idealized as either spheres or flat disks.

Spherical Particles

Consider two spherical particles of radius R in contact [Fig. 1(a)]. The water meniscus between them is bound by the two particles and by an imaginary torus. The small radius of this doughnut shaped torus is r_1, and the distance from the center to the inside wall of the torus is r_2 (this is the inner radius of the torus; it is a negative value in the case of a torus). From geometric considerations

$$(R + r_1)^2 = R^2 + (r_1 + r_2)^2 \tag{5a}$$

Hence

$$r_1 = \frac{r_2^2}{(2R - 2r_2)} \tag{5b}$$

The selection of the torus geometry implies several assumptions. First, the contact angle between the water and the surface of the particles is assumed to be zero and the particles are assumed to be perfectly smooth. Second, the effect of gravity on the geometry of the meniscus is ignored (i.e., the porewater pressure gradient is negligible relative to the average pressure). Finally, the torus is only a convenient approximation to the true geometry of the meniscus, amenable to analytical computations. Indeed, constant pressure in the water implies constant mean curvature according to Laplace's relation, yet the radius of curvature r_2 varies along the surface of the torus while the r_1 curvature is constant [Fig. 1(a)]. In fact, the correct geometry approaches a catenoid. Nevertheless, parameters computed using the torus geometry are similar to numerical results obtained with catenoids. Fisher (1926) showed the error to be small at low water contents, increasing up to 2% at the limit of the pendular regime (Gili 1988).

Eq. 2 can be rewritten in terms of α, the ratio of r_2 to R, by substituting (5) into (2)

$$\Delta u = (u_a - u_w) = \frac{T_s}{R\alpha}\left(\frac{2}{\alpha} - 3\right) \tag{6}$$

The force that the meniscus produces on the particle must include not only the pressure of the water acting on the cross-sectional area of the meniscus (i.e., matric suction) but the surface tension acting along the perimeter [Fig. 1(b)]. So the force F between two particles becomes

$$F = \Delta u(\pi r_2^2) + T_s(2\pi r_2) \tag{7}$$

The force contributed by the surface tension along the perimeter has been disregarded by several authors, even though this omission was highlighted as early as 1926 by Fisher. Its importance increases with water content (within the geometric limits of meniscus-based analysis) e.g., for $w = 0.02$ the error is 250%, and for $w = 0.04$ the error is 400%.

The equivalent effective stress σ'_{eq} due to capillarity can be estimated for a given particle packing. In the case of a simple cubic (SC) packing (coordination number 6, void ratio 0.91), the force F is spread over the effective area occupied by a particle $4R^2$. Combining results from (6) and (7), the equivalent effective stress becomes

$$\text{SC } \sigma'_{eq} = \frac{F}{4R^2} = \frac{\pi T_s}{4R}(2 - \alpha) \tag{8}$$

Meanwhile, considering the geometry of the meniscus between two particles, the volume of the meniscus can be calculated in terms of particle diameter and the meniscus's radii. Furthermore, the volume calculated can be related to the water content w. For the SC packing, the water content becomes

$$\text{SC } w = \frac{9}{8G_s}\left(\frac{\alpha^4}{1 - \alpha^2}\right)\left[1 - \frac{\alpha(2 - \alpha)}{2(1 - \alpha)}\arcsin\left(\frac{2(1 - \alpha)}{\alpha^2 + 2(1 - \alpha)}\right)\right] \tag{9}$$

where G_s = specific gravity [the complete derivation of equations presented in this paper and associated parametric studies can be found in Cho and Santamarina (1999)]. For small values of α, the first order Taylor expansion of (9) becomes

$$\text{SC } w = \frac{9\alpha^4}{8G_s} \tag{10}$$

Finally, the equivalent effective stress due to capillarity can be expressed in terms of the water content. Using the approximation for w, (8) becomes

$$\text{SC } \sigma'_{eq} = \frac{\pi T_s}{4R}\left[2 - \left(\frac{8}{9}G_s w\right)^{1/4}\right] \tag{11}$$

The geometric restrictions for the torus geometry and the pendular regime correspond to a water content $w \leq 0.063$ for the SC packing regardless of the grain size R.

A similar analysis can be applied to a tetrahedral (TH) packing (coordination number 12, void ratio 0.34). For the same size of the menisci $\alpha = r_2/R$ the water content in a tetrahedral packing is twice the water content in a simple cubic packing

$$\text{TH } [w(\alpha)]_{TH} = 2[w(\alpha)]_{SC} \tag{12}$$

The equivalent effective stress in this case is

$$\text{TH } [\sigma'_{eq}]_{TH} = 2\sqrt{2}[\sigma'_{eq}]_{SC} \tag{13}$$

The geometric restrictions for the torus geometry and the pendular regime correspond to a water content $w \leq 0.032$ for the tetrahedral packing. It is important to note that the soil structure for uniformly graded sands at the microscale can be constrained between the simple cubic packing and the tetrahedral packing.

The distribution of water is not necessarily homogeneous in an unsaturated soil. The normalized vapor pressure P/P_0, computed with Kelvin's equation is plotted in Fig. 2 versus the water content w for different particle sizes R, i.e., SC packing is assumed; radii are expressed in terms of water content as per (10). It can be seen that at the same vapor pressure (assumed homogeneous in the soil mass), the water content in-

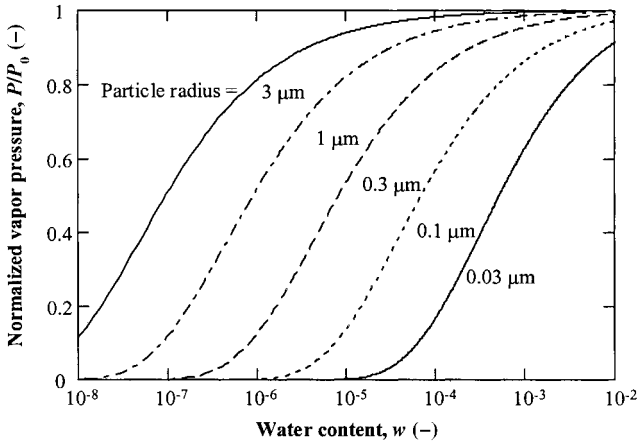

FIG. 2. Relationship between Normalized Vapor Pressure, Water Content, and Particle Size

creases with decreasing particle size. Therefore, the spatial variation in local water content (pendular regime) will reflect the spatial variation in local grain size distribution.

Modification for Hertzian Contact Area

The previous solution presumes that the area of the contact itself is nil. However, the capillary force and externally applied stresses cause the particles to deform. What is the magnitude of this effect? Let us consider two spheres of equal radius. Upon the application of a normal contact force F the contact point becomes a flat circular area of contact radius a. The size of this contact area depends on the shear modulus G and Poisson's ratio ν of the material of the particle, and on the radius R of the sphere, as predicted by Hertz theory

$$a = \sqrt[3]{\frac{3(1-\nu)}{8G} FR} \tag{14}$$

In an unsaturated soil, the area affected by the meniscus becomes altered by the area of the contact, as does the curvature r_1 for a given volume of water in the meniscus. There is no exact solution for this problem, and an iterative procedure is required: (1) The stress is computed taking into consideration capillary forces; (2) the area of the Hertzian contact is computed with (14); (3) the capillary force is recalculated taking into consideration the reduction in the cross section of the meniscus; and (4) a new value of stress is obtained. The procedure is repeated until the computed stress converges. In Fig. 3, the equivalent combined stress (i.e., sum of the equivalent effective stress due to capillarity and the applied stress due to external confinement) in the unsaturated soil is plotted versus the applied stress. The particle size (R = 1 μm), the particle stiffness (G = 3.7 GPa), and the degree of saturation ($S = 3 \cdot 10^{-6}$) for simple cubic packing were selected to highlight the effect. The lower dotted line is the 1:1 relation for a dry soil, i.e., with no capillary forces. The upper dashed line includes the effect of external confinement and the effect of capillarity uncorrected for contact area. The continuous line is the corrected solution obtained with the iterative procedure to correct for contact area. Results show the increased effect of capillarity at low confinement, and the vanishing effect of capillarity at high confining stress.

Flat Particles

If plate particles are analyzed as disks with radius $r_2 \gg r_1$ [Fig. 1(c)], the term $1/r_2$ can be neglected in Laplace's equation [(2)]. The suction pressure then becomes a function of the radius r_1. On the other hand, the separation distance between two particles t is twice the radius r_1. Hence, the water content w in equally spaced parallel plates is

$$w = \frac{W_w}{W_s} = \frac{A(2r_1)\gamma_w}{W_s} = \left(\frac{2A}{W_s/g}\right) r_1 \frac{\gamma_w}{g} = S_s r_1 \frac{\gamma_w}{g} \tag{15}$$

where W_w and W_s = weights of water and solid, respectively; A = surface area of one plate; γ_w = unit weight of water; S_s = specific surface; and g = acceleration due to gravity. Solving (15) for r_1 and replacing in Laplace's equation, the suction pressure Δu becomes

$$\Delta u = T_s \left(\frac{1}{r_1}\right) = T_s \left(\frac{S_s \gamma_w}{wg}\right) \tag{16}$$

For this disk geometry, the equivalent effective stress contributed by capillarity is $\pi/4$ of the suction pressure (the force component due to the surface tension also vanishes when $r_2 \gg r_1$). Particle size is not present in this equation. Instead, specific surface appears as a more meaningful parameter in the context of small platy particles. The effect of small, high-specific surface particles on capillarity has been recognized in the development of empirical equations in terms of D_{10} [e.g., Terzaghi and Peck (1948)].

As water dries, either the particles move closer together (i.e., smaller r_1) or the meniscus recedes between the particles at constant r_1. The parallel particle model applies to dispersed-aggregated systems (e.g., face-to-face contact). The analysis of flocculated fabrics with edge-to-face contacts leads to a lesser effect of capillarity on interparticle forces. While the previous analysis considers only the force contributed by capillarity on perfectly smooth disks, the analysis of equilibrium must also include the localized reaction at asperities and interparticle electrical forces (Nagaraj and Srinivasa Murthy 1985; Fam and Santamarina 1996).

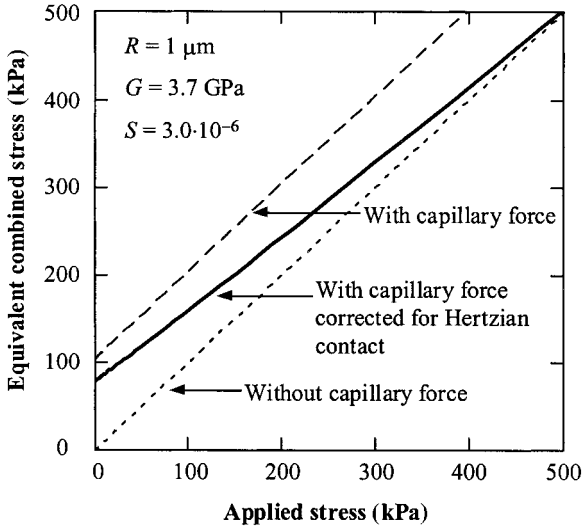

FIG. 3. Combined Stress Taking into Consideration Applied Effective Stress and the Contact-Level Capillary Force

RESULTS AND DISCUSSION

Fig. 4 shows the variation in equivalent effective stress due to capillarity versus the water content for both spherical and disk-shaped particles (G_s = 2.65) [(11), (13), and (16)]. The equivalent effective stress increases with decreasing water content, decreasing particle size, increasing specific surface, and increasing coordination.

Note the relatively limited sensitivity of the equivalent effective stress to water content in spherical particles as compared to flat particles. Indeed, as the water content decreases, the negative pressure in the meniscus increases drastically, but the effective area of the meniscus between spherical particles decreases as well. On the other hand, the effective area in flat particles remains constant, assuming that particles move closer together.

Several restrictions of the models are identified in the figure. The geometric limits (① and ①′) are derived from the torus geometry. The limit for cavitation (②) is also shown; the location of this boundary depends on the assumed cavitation pressure for the fluid (for illustration, a cavitation pressure of 1 MPa is selected). The equivalent effective stress contributed by capillarity will disappear when the negative pressure exceeds the cavitation pressure. The upper limit (③) shown for flat particles corresponds to an interparticle distance ($2 \cdot r_1$) equal to ten times the molecular diameter in (16).

There are other factors in real soils that increase strength and stiffness at low saturation. As water dries, fines migrate to contacts, and form buttresses between larger particles. These buttresses increase the stiffness of the granular skeleton formed by the coarser grains. At the same time, the ionic concentration in the pendular water increases and eventually

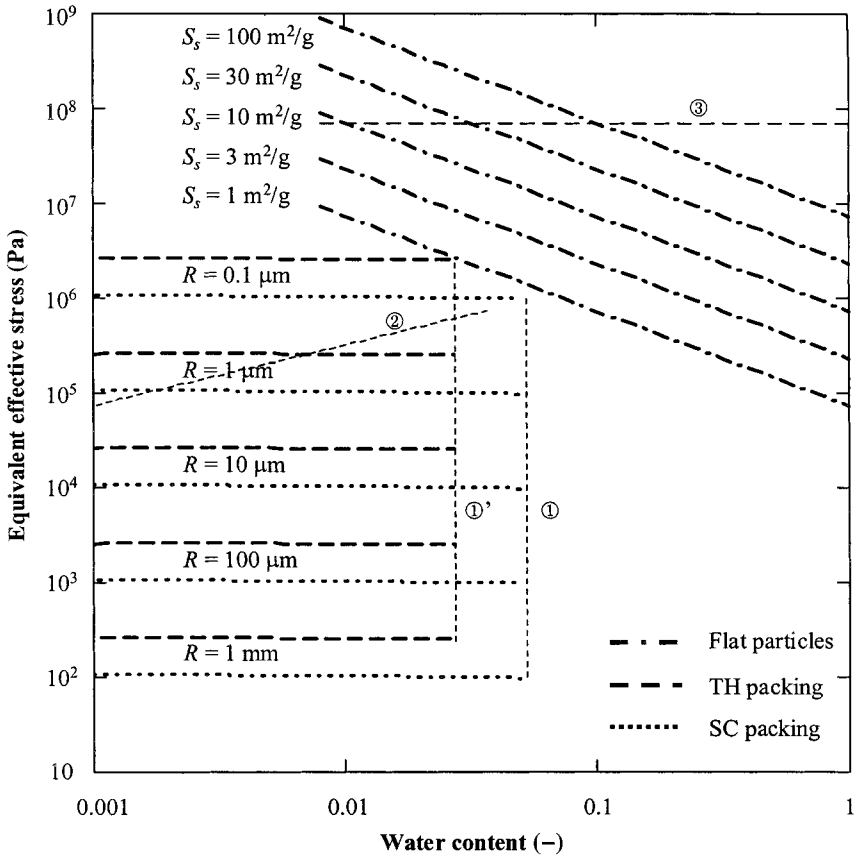

FIG. 4. Equivalent Effective Stress versus Gravimetric Water Content

reaches saturation causing the precipitation of salt crystals between the two contacting particles. Salt precipitation also increases the stiffness of the particulate skeleton. This phenomenon is readily seen with optical microscopy by observing the desiccation of a saltwater meniscus between two glass bead particles. Finally, two particles can become ionically bonded at low water content (e.g., a calcium ion Ca^{++} can bond two negative charges on the surfaces of contacting particles). It is expected that these phenomena produce effects similar to cementation; this is the case of loess (Rinaldi et al. 1998).

SMALL STRAIN STIFFNESS

The shear wave velocity V_s in a homogeneous, isotropic continuum can be expressed in terms of shear modulus G and mass density ρ

$$V_s = \sqrt{\frac{G}{\rho}} \tag{17}$$

The shear modulus in particulate materials depends on the effective interparticle contact forces and the ensuing contact stiffness. As shown above, the presence of water in unsaturated particulate materials increases the contact forces, but it also increases the density of the medium.

Previous Studies

The effect of capillarity on the shear-wave velocity in soils was studied by Wu et al. (1984) and Qian et al. (1991, 1993). In those studies, sands were mixed with distilled water to a preselected degree of saturation. The mixture was placed in an airtight container and stored for at least 24 h to ensure uniform water distribution. Specimens were then prepared by compacting the wet soil to the required void ratio, and tested in a resonant column. Wu et al. (1984) obtained an empirical equation to predict the optimum degree of saturation (S_{opt}) corresponding to the peak of the shear-wave velocity V_s

$$S_{opt} = [-6.5 \log(D_{10}) + 1.5]/100 \tag{18}$$

where D_{10} = 10% effective grain size (mm). However, it is clearly observed under optical microscopy that two surface-wet particles do not form a meniscus when brought into contact unless the water film is fairly thick. Therefore, the specimen preparation method followed by Wu et al. (1984) and Qian et al. (1991, 1993) is adequate to study freshly remolded unsaturated soils, but it does not apply to soils that have been subjected to gradual drying. Thus, the applicability of (18) should be restricted to freshly remolded soils.

Experimental Device and Procedure

In order to explore the implications of capillarity on stiffness at low water contents without remolding the specimen, drying tests were performed while monitoring the specimen with shear waves. The oedometric cell described in Fam and Santamarina (1995) was modified for this purpose [Fig. 5(a)]. The cell diameter and height were selected as a compromise between accuracy in travel time measurements, side friction, and duration of drying. The Plexiglas shell, the Plexiglas base, and the brass upper plate (weight 11.8 N; applied vertical effective stress = 1.5 kPa) were all machined within 0.05 mm tolerance. The Plexiglas shell was perforated, and a cotton threadlike wick was installed in each hole to facilitate evaporation and to favor a homogeneous water distribution. Piezocrystal bender elements (Morgan Matroc Inc., Bedford, Ohio) were mounted on the top and bottom platens to send and to receive shear waves. Crystals were insulated with a double coating of polyurethane, and encapsulated inside resin to fix them to the platens.

The experimental setup is shown in Fig. 5(b). A Krohn-Hite Signal Generator Model 1400A was used to feed a square

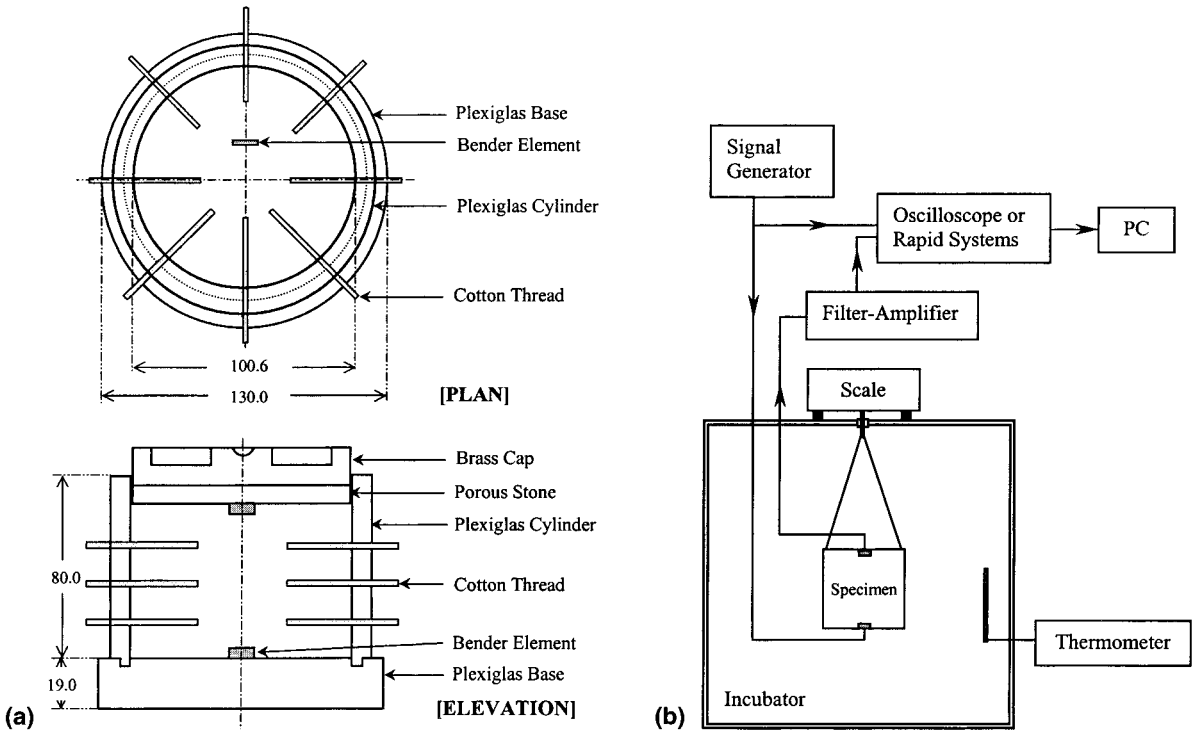

FIG. 5. (a) Schematic Cell Design (All Dimensions in Millimeters); (b) Experimental Setup

TABLE 1. Tested Materials—Properties

Material (1)	Glass bead (2)	Kaolinite (3)	Granite powder (4)	Sandboil sand (5)
D_{10} (μm)	260	1	17	170
D_{50} (μm)	320	5	89	360
Specific gravity	2.46	2.70	2.75	2.62
Specific surface (m^2/g)	10^{-2} [a]	13[b]	1.5[b]	1.1[b]

[a]Data estimated from particle size.
[b]Calibrated absorption methods.

TABLE 2. Composition, Void Ratio, and Test Type for Each Specimen

Specimen (1)	Composition of Materials: Glass bead (%) (2)	Kaolinite (%) (3)	Granite powder (%) (4)	Sandboil sand (%) (5)	Void ratio (6)	Test type (7)
I	100	—	—	—	0.601	Drying
II	80	20	—	—	0.564	Drying
III	—	—	100	—	0.692	Drying
IV	—	—	—	100	0.507	Drying
V	100	—	—	—	0.553	Recovery

pulse to the lower bender element. Signals detected with the upper crystal were amplified with a Krohn-Hite Multi Channel Filter-Amplifer Model 3364, and digitized with a Rapid Systems digital storage oscilloscope Model R1016. The average of 256 stacked signals was stored in a personal computer.

The tested specimens included glass beads (spherical particles), a mixture of glass beads and kaolinite (flat particles; clay), granite powder (angular particles; silt), and sand obtained from a liquefied site in Blytheville, Arkansas (sandboil sand). Tables 1 and 2 summarize relevant information for these materials used and the tested specimens. Particle size distributions are shown in Fig. 6; these plots have been purposely rotated 90° to facilitate comparison with other results. Glass beads were used to approximate the theoretical model [(5)–(14)]. The mixture of glass beads and kaolinite was used to increase the specific surface; the resulting specimen has a pronounced gap-graded distribution. Granite powder is a byproduct of rock crushing during the production of aggregates for concrete, and it is a well-graded material composed of angular grains (C_c = 1.1; C_u = 6.2). The sandboil sand is a natural soil from a paleoliquefaction site in mid-America.

The materials were mixed with distilled water at saturated conditions, and gradually poured into the cell. Kneading facilitated the densification of materials and the removal of air bubbles. Glass beads were extensively washed in deionized water to avoid salt precipitation at low water contents.

Tests were run in an incubator at 50°C to speed drying. Temperature was kept constant to avoid changes in surface tension (surface tension decreases with increasing temperature), and changes in confinement due to the expansion and shrinkage of the cell. The specimen was suspended with a wire inside the incubator. The wire acted on an external scale that allowed the weight of the specimen to be monitored, in order to compute the water content or the degree of saturation.

The measured shear-wave velocity is plotted versus the corresponding degree of saturation in Fig. 7. When the degree of saturation decreases from the saturated condition (S = 1.0) to the dry condition (S = 0), the shear-wave velocity increases in all specimens. A detailed discussion follows for each material.

Results for Clean Glass Beads

The shear-wave velocity in the glass bead specimen reaches a peak and decreases abruptly as drying continues [Fig. 7(a)]. In the ideal case of spherical particles and constant fabric, the shear-wave velocity is proportional to the effective stress as $V_s \propto \sigma'^{1/6}$ (Hertzian contact). Therefore, the trend $V_s - S$ is smoother than the suction-saturation trend. Pore size governs the magnitude of the effective stress increase in the region of funicular water. The gentle slope between points A and B suggests monosized pores. Indeed, it is unlikely that a uniform coarse-grained soil will form a dual porosity medium.

The negative pore-water pressure in the pendular region (to the left of point B) causes a strong increase in shear-wave

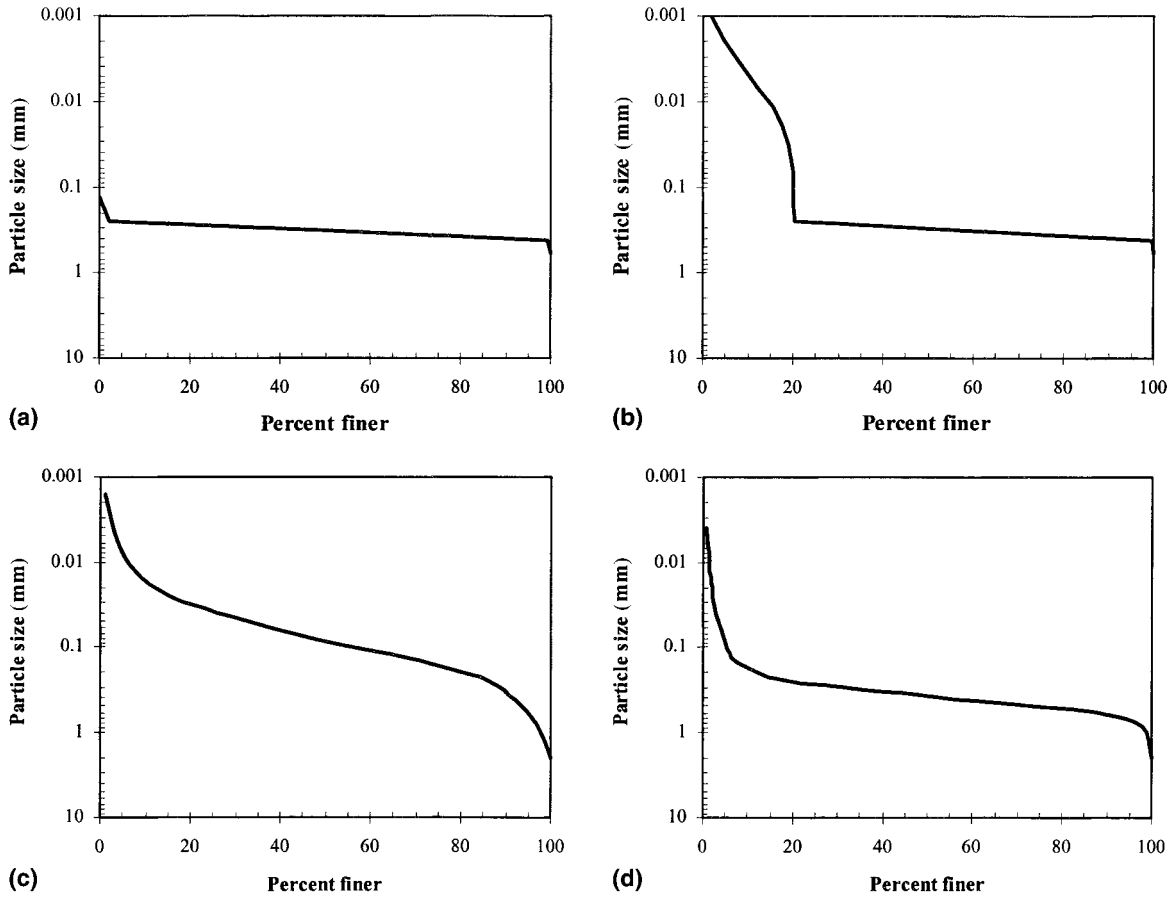

FIG. 6. Particle Size Distributions for Different Materials: (a) Glass Beads; (b) Mixture of Kaolinite and Glass Beads; (c) Granite Powder; (d) Sandboil Sand

velocity. The degree of saturation at peak shear-wave velocity is $S = 0.007$. For comparison, for freshly remolded specimens (18) predicts the peak in stiffness at $S_{opt} = 0.053$. The drop in stiffness between the peak and the perfectly dry state may reflect several internal mechanisms. For example, menisci may form between particles that remain separated by a short distance; as water evaporates, menisci between noncontacting particles fail earlier than menisci between particles in contact (a similar analysis could be extended to the effect of surface roughness). Therefore, the loss in equivalent effective stress contributed by capillarity is a gradual process that starts before the specimen is completely dry, even if particles are of uniform size. Finally, the difference between the velocities at $S = 0$ and at $S = 1.0$ cannot be fully accounted for by changes in mass density. An increase in internal coordination during drying and residual compressive stress are expected.

Results for Kaolinite-Glass Beads

The shear wave velocity in the kaolin-glass beads specimen increases in three distinct steps and shows no drop even at the dry condition [Fig. 7(b)]. In fact, the shear-wave velocity at $S = 0$ is 18 times larger than the velocity at $S = 1.0$. The empirical equation for remolded specimens [(18)] predicts a peak in stiffness at an optimal saturation of $S_{opt} = 0.21$. The measured shear-wave velocity almost doubles between $S_{opt} = 0.21$ and $S = 0$ in this undisturbed specimen. The specimen did not develop any crack and the observed shrinkage was negligible. Clearly, glass beads formed a granular skeleton that prevented shrinkage and cracking of the specimen. When the specimen was sectioned after the test, quasi-spherical cavities, like bubbles, could be seen throughout, and clay particles had moved toward glass bead contacts. Clay-based strengthening of contacts, bonding due to ion sharing, and salt precipitation are expected as drying proceeds beyond point C to the peak velocity at $S = 0$.

Results for Granite Powder

The shear-wave velocity in the granite powder specimen increases continuously and shows no drop even at the perfectly dry condition $S = 0$ [Fig. 7(c)]. The shear-wave velocity for the dry specimen is approximately eight times larger than for the saturated specimen. It is expected that stiffening mechanisms at low saturation may explain the jump in shear-wave velocity near $S = 0$ in this specimen as well, i.e., fines migration to contacts, salt precipitation, and bonding. When the specimen is resaturated by flooding, the shear wave velocity drops to its initial value [square points in Fig. 7(c)]. This result suggests that the light cementation that develops during drying disappears upon wetting.

The optimum degree of saturation calculated with the empirical relation for remolded specimens [(18)] predicts the peak in stiffness for the granite powder specimen at $S_{opt} = 0.11$. However, the measured peak shear-wave velocity in the undisturbed specimen is 1.7 times greater than that at $S_{opt} = 0.11$.

Results for Sandboil Sand

The shear-wave velocity for the sandboil sand specimen increases continuously and shows no drop even at the perfectly dry condition $S = 0$ [Fig. 7(d)]. The shear-wave velocity for the dry sand is nearly two times greater than for the saturated sand. The optimum degree of saturation calculated with (18) is $S_{opt} = 0.065$. The measured peak shear-wave velocity in the undisturbed specimen is 1.6 times greater than the shear-wave velocity at S_{opt}.

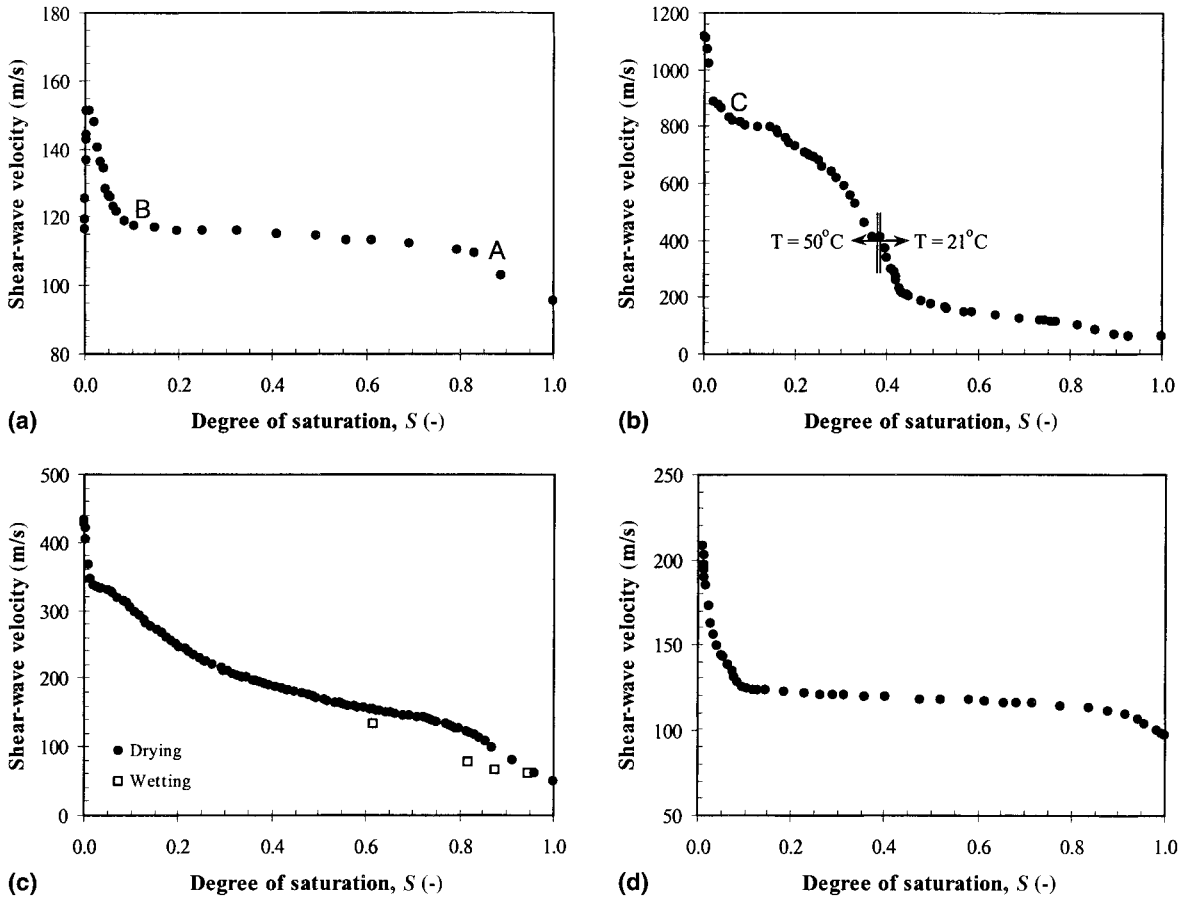

FIG. 7. Shear-Wave Velocity versus Degree of Saturation for Different Materials: (a) Clean Glass Beads (Deionized Water); (b) Mixture of Kaolinite and Glass Beads; (c) Granite Powder; (d) Sandboil Sand

Comparison between Microscale-Based Predictions and Experimental Results

Empirical expressions for shear-wave velocity V_s have been proposed for particulate materials in terms of the state of effective stress (Stokoe et al. 1991; Santamarina and Cascante 1996)

$$V_s = \theta \left(\frac{\sigma'_v + \sigma'_h}{2p_a} \right)^{\beta} \tag{19}$$

where θ and β = empirical parameters; σ'_v and σ'_h = vertical and horizontal effective stress, respectively; and p_a = atmospheric pressure used for dimensionality. Suggested values for β are (Santamarina and Aloufi 1999): $\beta = 1/6$ for Hertzian contact, $\beta = 1/4$ for plastic spherical contact and for cone-to-phase contact (angular or rough particles), $\beta \cong 0.2$ to 0.25 for sands (the looser the sand the higher β), and $\beta \cong 0.27$ to 0.30 for kaolin.

Eq. (19) is used to compute the shear-wave velocity at a given saturation S, $[V_s]_S$, in terms of the shear-wave velocity at saturation $S = 1.0$, $[V_s]_{S=1}$, taking into consideration the changes in mass density [for saturated conditions in an oedometer $\sigma'_v + \sigma'_h = (1 + K_0)\sigma'_v$, while σ'_{eq} due to capillarity is considered isotropic]

$$[V_s]_S = [V_s]_{S=1} \left[1 + \frac{2\sigma'_{eq}}{(1 + K_0)\sigma'_v} \right]^{\beta} \sqrt{\frac{e + G_s}{eS + G_s}} \tag{20}$$

where σ'_{eq} = equivalent effective stress due to capillarity at a given degree of saturation S; e = void ratio; G_s = specific gravity; and K_0 = coefficient of lateral earth pressure at rest. Hence, the shear-wave velocity at a given saturation S can be predicted from the shear-wave velocity at saturation $S = 1.0$ by knowing the parameter β and estimating σ'_{eq} using either the spherical or the flat particle models.

The shear-wave velocities predicted with (20) for the four specimens at three levels of saturation (i.e., $S = 0.05$, 0.1, and 0.15) are compared against the measured values in Fig. 8. The coefficient of lateral earth pressure was assumed to be $K_0 = 1 - \sin\phi$ in this analysis. Measured values for the glass beads and the sandboil sand specimens are well predicted using the spherical particle model, and $\beta = 1/6$ for the glass beads and $\beta = 0.22$ for the sandboil sand. However, since the finer fraction has an important role in the global stiffness, measured

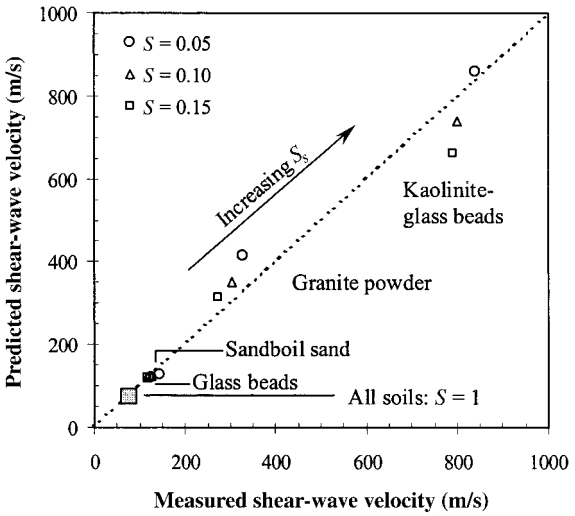

FIG. 8. Comparison between Measured and Predicted Shear-Wave Velocities

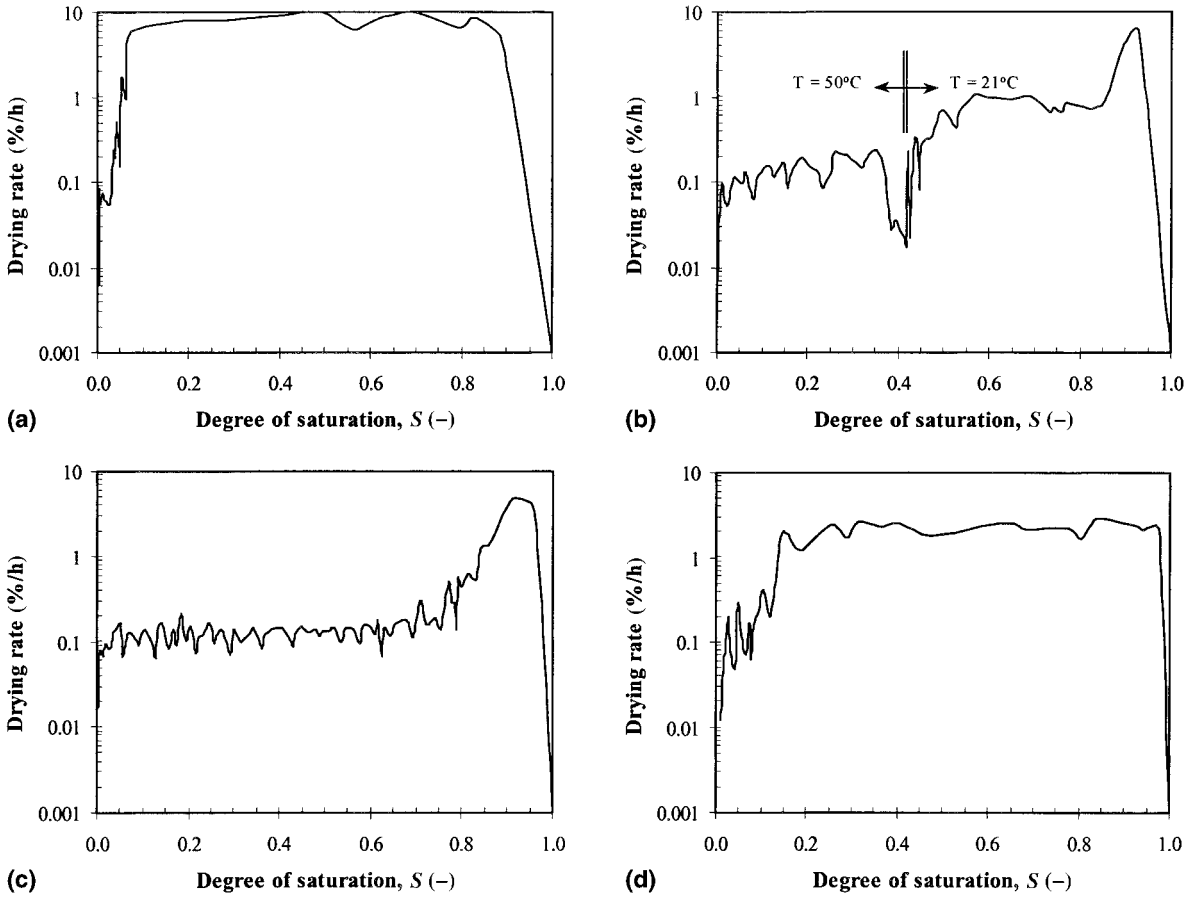

FIG. 9. Drying Rate versus Degree of Saturation in Incubator at 50°C for Different Materials: (a) Clean Glass Beads (Deionized Water); (b) Mixture of Kaolinite and Glass Beads; (c) Granite Powder; (d) Sandboil Sand

velocities for the kaolinite-glass beads and the granite powder specimens cannot be explained by the spherical particle model. Predictions shown in Fig. 8 correspond to the flat particle model, and $\beta = 0.27$ for kaolinite-glass beads and $\beta = 0.24$ for granite powder.

The maximum shear wave velocity $[V_s]_{max}$ that is reached by these specimens (at $S = 0$) can be estimated as

$$[V_s]_{max} = 2{,}200/\sqrt{D_{10}} \quad (\text{for } 5\ \mu\text{m} \leq D_{10} \leq 300\ \mu\text{m}) \qquad (21)$$

where $[V_s]_{max}$ is in meters per second; and D_{10} is in micrometers.

The parallelism between the grain-size distribution plots (Fig. 6) and the shear-wave velocity plots (Fig. 7) is noticeable, highlighting the importance of grain-size distribution on capillarity. A similar observation has been made in the context of water retention curves [e.g., Öberg (1997)].

Drying Rates

For completeness, Fig. 9 presents the change in drying rate ($\partial S/\partial t$) versus the degree of saturation for the three specimens. Three general regions are observed. At the beginning, near saturation $S = 1.0$, the drying rate increases reflecting the increase in temperature within the specimen as it warms up toward the incubator temperature. After air entry, evaporation occurs at an almost constant rate for uniform pore-size specimens. Finally, the evaporation of water within small menisci and loosely bound water near saturation $S = 0$ takes place at a decreasing rate (Santamarina and Wakim 1992; Kayyal 1995; Knight et al. 1996).

EXPERIMENTAL STUDY OF MENISCI FAILURE AND RECOVERY

Shear deformation involves particle displacement and particle rotation. When an unsaturated soil is subjected to shear, menisci are strained and may eventually break causing a reduction in the capillary effect. When the strain in a soil exceeds the strain that menisci can sustain, both soil strength and stiffness are affected. The purpose of this study is to determine the strain at menisci failure and its dependency on water content, by performing microscale tests and analyses. Then, an assessment of menisci regeneration is attempted.

Menisci Failure

Microscale tests were conducted with two glass beads (diameter $D = 1.6$ mm) under optical microscopy ($\times 150$). The glass beads were cleaned with distilled water before testing. Measurements included the initial radii of the meniscus, i.e., r_1 and r_2 in Fig. 1(a), and the relative position of the particles

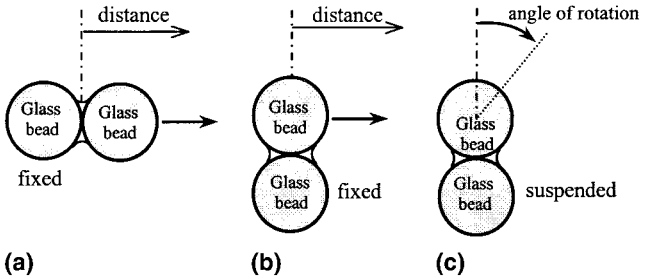

FIG. 10. Sketch of Microscale Tests for Menisci Failure: (a) Pulling Test; (b) Horizontal Shear Test; (c) Rotating Test

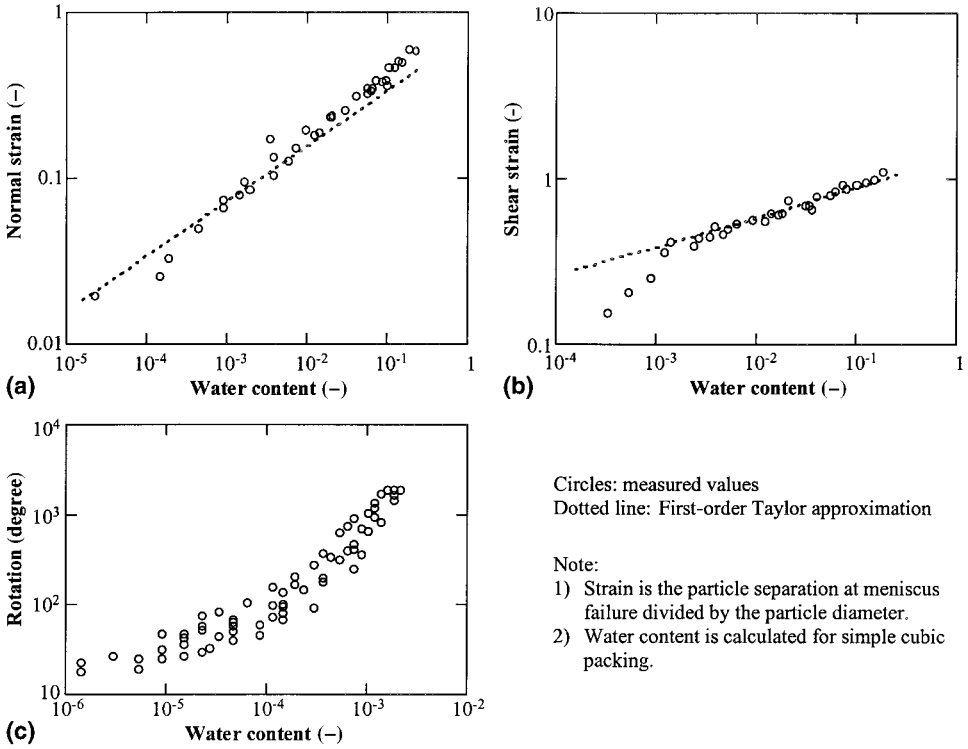

FIG. 11. Microscale Test for Menisci Failure Showing Experimental and Analytical Results: (a) Pulling Test; (b) Horizontal Shear Test; (c) Rotating Test

at menisci failure. The measured radii were used to compute the water content by using (9) or (10) (SC packing, coordination number 6), and the particle positions at menisci failure were used to compute the equivalent strain.

Microscale tests for menisci failure are sketched in Fig. 10. Three tests were run: (1) Pulling along the normal-contact direction; (2) shearing parallel to the contact plane; and (3) rotation of one particle relative to the other while maintaining interparticle contact. Results for the three cases are shown in Fig. 11. Each circle represents a separate test. The trends show that the strain when menisci fail decreases with the decrease in water content in the three cases.

An analytical microscale solution was developed to predict the strain at meniscus failure for the cases of normal and shear tensile deformations (Cho and Santamarina 1999). The analysis is based on estimating the zero-suction condition that develops when a meniscus is strained and its radii r_1 and r_2 change correspondingly. For a given strain, the volume of water can be expressed in terms of radii r_1 and r_2, and the particle radius R. The water content can be related to the volume of water for SC packing. The first-order Taylor approximation for the normal strain (i.e., pulling test) is

$$\varepsilon_a = \frac{\delta}{2R} \approx 0.53(Se)^{1/3} = 0.53(G_s w)^{1/3} \tag{22}$$

where ε_a = normal strain (i.e., axial strain); δ = distance between two particles when meniscus fails; R = particle radius; S = degree of saturation; e = void ratio; G_s = specific gravity of particle; and w = water content. The first-order Taylor approximation for the shear strain in the horizontal shear test can be expressed in terms of the normal strain

$$\varepsilon_s = \sqrt{\varepsilon_a^2 + 2\varepsilon_a} \tag{23}$$

where ε_s = shear strain.

Analytical predictions are superimposed on Figs. 11(a and b). In general, there is good agreement between experimental data and analytical predictions. The gap at relatively high water content reflects the nontoroidal shape of the stretched me-

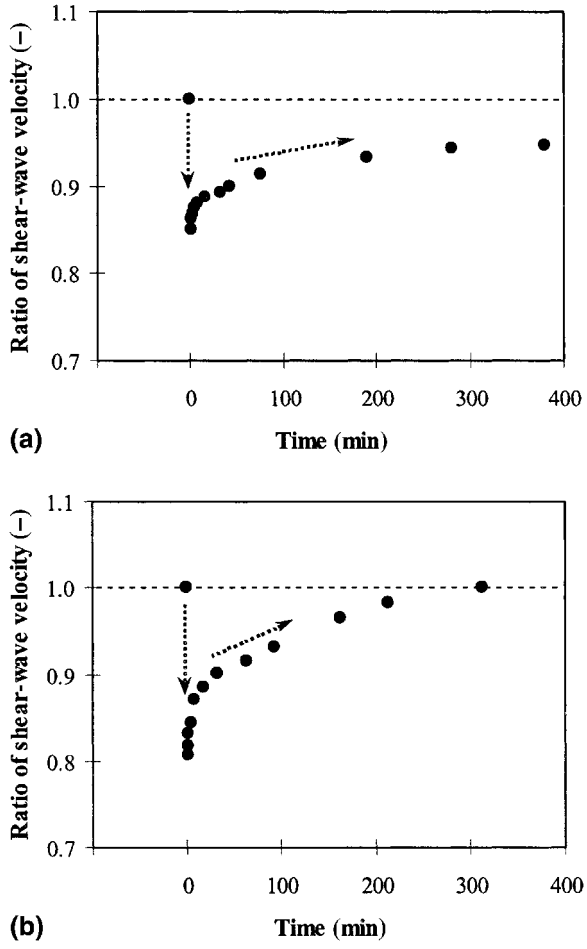

FIG. 12. Perturbation-Recovery Test; Note Shear-Wave Velocity Is Normalized with Respect to Shear-Wave Velocity Immediately before Impact: (a) *S* = 0.40 Degree of Saturation; (b) *S* = 0.01 Degree of Saturation

niscus. On the other hand, deviations at small water content may reflect experimental difficulties related with measuring and preserving very small menisci.

The observed strains for menisci failure ($\varepsilon = 0.01$ to 1) are higher than the threshold strain for sands determined from the shear modulus degradation curves. Therefore, capillary effects will contribute to low strain stiffness, as shown earlier. Yet, small menisci (low water content) may fail before soils reach the strain at peak strength and will not contribute to soil strength [$w \approx 0.01$ or lower, from (22) or (23)]. For higher water contents, capillary forces will contribute to increase both the low strain stiffness of soils and the strength of the soil.

It is important to note that the negative pressure gradually decreases as the meniscus is deformed, due to the changes in curvature that it experiences (Laplace's equation). In other words, the contribution of a meniscus to the internal forces does not vanish suddenly, but gradually with the strain level. Early experimental results by Donald (1956) and Escario and Jucá (1989) support these observations. Limiting values of water content w must be taken into consideration when applying models for the shear strength of unsaturated soils; Rahardjo and Han (1995) show ϕ varying with S.

Suction Homogenization and Menisci Recovery

Perturbations may alter the internal equilibrium at the macroscale, even if menisci failure does not take place. To explore this suspicion, a specimen was laterally impacted with a pendulum to deliver a fixed impulse (Specimen V in Table 2). The shear-wave velocity was measured before and after impact. The study was repeated at different degrees of saturation while the degree of saturation remained approximately constant during each study. Data are plotted in Fig. 12 for the degree of saturation $S = 0.4$, i.e., funicular stage—pressure diffusion-based homogenization, and for $S = 0.01$, i.e., pendular stage—vapor pressure-based homogenization. Results show fast and complete recovery in the funicular stage. On the other hand, the rate of recovery is low in the pendular stage, and full recovery may not be reached. These results show a potential mechanism to explain thixotropic recovery in unsaturated materials (Díaz Rodríguez and Santamarina 1999).

SUMMARY AND CONCLUSIONS

Experiments and analyses were performed to gain further insight into the microscale behavior of unsaturated particulate materials. Emphasis was placed on the pendular stage and on the effect of capillary forces on small strain stiffness. Other factors, besides capillarity, coexist and increase the stiffness at low saturation levels. Fig. 13 summarizes particle-level phenomena identified in this study. The main conclusions from this study follow:

- The contribution of capillarity to interparticle forces in-

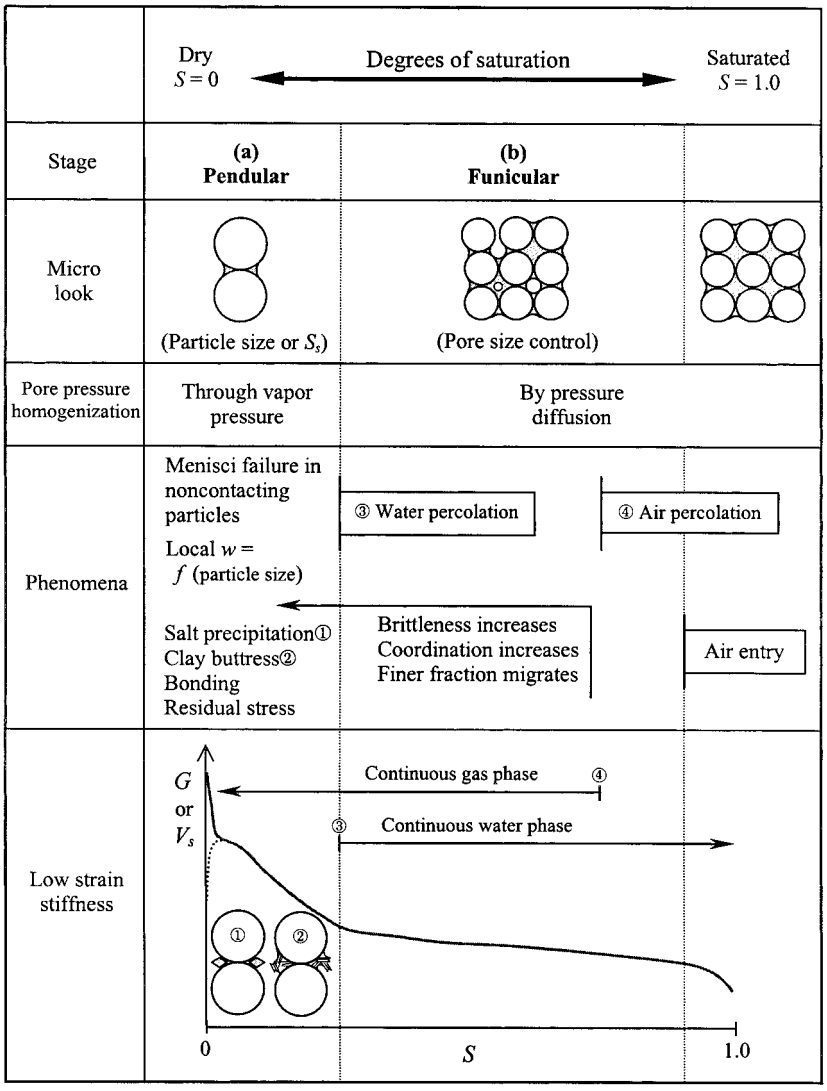

FIG. 13. Stages of Unsaturated Conditions and Related Phenomena

volves not only matric suction (i.e., negative pore-water pressure) but the surface tension force along the edge of menisci, as well.
- The ''equivalent effective stress'' due to capillary forces increases with decreasing water content, decreasing particle size, and increasing coordination. Specific surface is a meaningful parameter in the characterization of unsaturated soils.
- Shear waves permit studying the evolution of effective interparticle forces. This is particularly valuable in the pendular regime where direct measurement of the negative pore-water pressure is not feasible. Remolding is not an appropriate specimen-preparation procedure to study the behavior of low water-content soils.
- The shear-wave velocity at low saturation can be estimated to a first approximation form the shear-wave velocity of the saturated specimen by taking into consideration particle size, shape, and water content.
- Grain size distribution plays a crucial role in the evolution of stiffness with saturation.
- An unsaturated soil shows a sudden drop in low strain stiffness when perturbed, followed by a time-dependent regain. The rate of regain is faster when menisci are interconnected (funicular stage). In the pendular stage, pore-water pressure homogenization takes place through the vapor pressure; this is a slow process and stiffness regain may not be complete.
- The strain at menisci failure decreases with the decrease in water content. Unless the water content is extremely small, menisci will fail at strains greater than the threshold strain of the soil; therefore, partial saturation is a stabilizing force for the soil skeleton. On the other hand, small menisci may fail before the strain at peak strength of soils (depending on the degree of saturation). Thus, capillary forces at low water contents cause an increase in the low strain stiffness of soils, but may not contribute to the peak strength.

ACKNOWLEDGMENTS

This study is supported by the Mid-America Earthquake Center, Urbana, Ill., under National Science Foundation Grant EEC-970185. E. Macari, L. Hoyos, and D. Muir Wood provided valuable information and comments. The authors are very thankful to reviewers for their detailed reviews. Specific surface data were gathered by K. A. Klein and Y.-H. Wang. Derivation and further analyses associated with this paper can be found on the authors' website, http://www.ce.gatech.edu/~carlos/Laboratory/public/electronic.html.

APPENDIX. REFERENCES

Aitchison, G. D. (1960). ''Relationships of moisture stress and effective stress functions in unsaturated soils.'' *Conf. British Nat. Soc. of Int. Soil Mech. and Found. Engrg.*, Butterworth's, London, 47–52.

Aitchison, G. D., and Donald, I. B. (1956). ''Effective stresses in unsaturated soils.'' *2nd Proc. of Australia-New Zealand Conf. on Soil Mech. and Found. Engrg.*, University of Melbourne, Australia, 192–199.

Aubertin, M., Ricard, J.-F., and Chapuis, R. P. (1998). ''A predictive model for the water retention curve: Application to tailings from hard-rock mines.'' *Can. Geotech. J.*, Ottawa, 35, 55–69.

Bear, J. (1979). *Hydraulics of groundwater*, McGraw-Hill, New York.

Bishop, A. W. (1959). ''The principle of effective stress.'' *Teknisk Ukeblad I Samarbeide Med Teknikk*, Oslo, Norway, 106(39), 859–863.

Bishop, A. W. (1961). ''The measurement of pore pressure in the triaxial test.'' *Conf. British Nat. Soc. of Int. Soil Mech. and Found. Engrg.*, Butterworth's, London, 38–46.

Bishop, A. W., and Blight, G. E. (1963). ''Some aspects of effective stress in saturated and partly saturated soils.'' *Géotechnique*, London, 13(3), 177–196.

Bishop, A. W., Kumapley, N. K., and El-Ruwayih, A. (1975). ''The influence of pore-water tension on the strength of clay.'' *Philosophical Trans. Royal Soc.*, London, 278(A.1286), 511–554.

Blight, G. E. (1967). ''Effective stress evaluation for unsaturated soils.'' *J. Soil Mech. and Found. Div.*, ASCE, 93(2), 125–148.

Cho, G. C., and Santamarina, J. C. (1999). ''Unsaturated particulate materials—Analytical study.'' ⟨http://www.ce.gatech.edu/~carlos/Laboratory/public/electonic.html⟩.

Defay, R., and Prigogine, I. (1966). *Surface tension and adsorption*, D. H. Everett, translator, Longman's, London.

Díaz-Rodríguez, J. A., and Santamarina, J. C. (1999). ''Thixotropy: The case of Mexico City soils.'' *XI Panamerican Conf. on Soil Mech. and Geotech. Engrg.*, 1, 441–448.

Donald, I. B. (1956). ''Shear strength measurements in unsaturated non-cohesive soils with negative pore pressures.'' *2nd Proc. of Australia-New Zealand Conf. on Soil Mech. and Found. Engrg.*, University of Melbourne, Australia, 200–204.

Escario, V., and Jucá, J. F. T. (1989). ''Strength and deformation of partly saturated soils.'' *Proc., Int. Conf. on Soil Mech. and Found. Engrg.*, Balkema, Rotterdam, The Netherlands, 1, 43–46.

Fam, M., and Santamarina, J. C. (1995). ''Study of geoprocesses with complementary wave measurements in an oedometer.'' *Geotech. Testing J.*, ASTM, 18(3), 307–314.

Fam, M., and Santamarina, J. C. (1996). ''Coupled diffusion-fabric-flow phenomena: An effective stress analysis.'' *Can. Geotech. J.*, Ottawa, 33, 515–522,

Fisher, E. A. (1923). ''Some factors affecting the evaporation of water from soil.'' *J. Agric. Sci.*, London, 13, 121–143.

Fisher, J. C. (1948). ''The fracture of liquids.'' *J. Appl. Phys.*, 19, 1062–1067.

Fisher, R. A. (1926). ''On the capillary forces in an ideal soil; Correction of formulae given by W. B. Haines.'' *J. Agric. Sci.*, London, 16, 492–505.

Fredlund, D. G. (1991). ''How negative can pore-water pressures get?'' *Geotech. News*, Vancouver, (Sept.), 44–46.

Fredlund, D. G., Morgenstern, N. R., and Widger, R. A. (1978). ''The shear strength of unsaturated soils.'' *Can Geotech. J.*, Ottawa, 15(3), 313–321.

Fredlund, D. G., and Rahardjo, H. (1993). *Soil mechanics for saturated soils*, Wiley, New York.

Giancoli, D. C. (1998). *Physics—Principles with application*, 5th Ed., Prentice-Hall, Englewood Cliffs, N.J.

Gili, J. A. (1988). ''Modelo Microstructural para Medios Granulares No Saturados.'' PhD thesis, Universidad Politechnica de Catalunya, Spain.

Gilliland, E. R. (1938). ''Fundamental of drying and air conditioning.'' *J. Industrial and Engrg. Chem.*, Washington, D.C., 30, 506–514.

Guan, Y., and Fredlund, D. G. (1997). ''Use of the tensile strength of water for the direct measurement of high soil suction.'' *Can. Geotech. J.*, Ottawa, 34(4), 604–614.

Hilf, J. W. (1956). ''An investigation of pore-water pressure in compacted cohesive soils.'' PhD thesis, U.S. Bureau of Reclamation, TC 654, University of Colorado, Boulder, Colo.

Hillel, D. (1980). *Applications of soil physics*, Academic, San Diego.

Kayyal, M. K. (1995). ''Effect of the moisture evaporative stages on the development of shrinkage cracks in soils.'' *Proc., 1st Int. Conf. on Unsaturated Soils*, E. E. Alonso and P. Delage, eds., Balkema, Paris, 373–379.

Knight, R., Tercier, P., and Goertz, D. (1996). ''A laboratory procedure for estimating irreducible water saturation from cuttings.'' *The Log Analyst*, (Jul.–Aug.), 18–24.

Kohgo, Y., Nakano, M., and Miyazaki, T. (1993). ''Theoretical aspects of constitutive modelling for unsaturated soils.'' *Soils and Found.*, Tokyo, 33(4), 49–63.

Leverson, S. M., and Lohnes, R. A. (1995). ''Moisture tension relations in sand.'' *Proc., 1st Int. Conf. on Unsaturated Soils*, E. E. Alonso and P. Delage, eds., Balkema, Paris, 387–392.

Marinho, F. A. M., and Chandler, R. J. (1995). ''Cavitation and the direct measurement of soil suction.'' *Proc., 1st Int. Conf. on Unsaturated Soils*, E. E. Alonso and P. Delage, eds., Balkema, Paris, 623–630.

Nagaraj, T. S., and Srinivasa Murthy, B. R. (1985). ''Compressibility of partly saturated soils.'' *J. Geotech. Engrg.*, ASCE, 111(7), 937–942.

Newitt, D. M., and Conway-Jones, J. M. (1958). ''A contribution to the theory and practice of granulation.'' *Trans. Inst. Chem. Engrg., Chem. Engrg. Res. and Des.*, Pergamon, U.K., 36, 422–442.

Öberg, A.-L. (1997). Matrix suction in silt and sand slopes—Significance and practical use in stability analysis.'' PhD thesis, Chalmers University of Technology, Göteborg, Sweden.

Oliver, T. R., and Newitt, D. M. (1949). ''The measurement of suction potentials and moisture distribution in drying granular soils.'' *Trans. Inst. Chem. Engrg.: Chem. Engrg. Res. and Des.*, Pergamon, U.K., 27, 9–18.

Pietsch, W. (1991). *Size enlargement by agglomeration*, Wiley, New York.

Qian, X., Gray, D. H., and Woods, R. D. (1991), ''Resonant column tests on partially saturated sands.'' *Geotech. Testing J.*, 14(3), 266–275.

Qian, X., Gray, D. H., and Woods, R. D. (1993). ''Voids and granulometry: Effects on shear modulus of unsaturated sands.'' *J. Geotech. Engrg.*, ASCE, 119(2), 295–314.

Rahardjo, H., and Han, K. K. (1995). ''Shear strength of unsaturated soils

as it applies to slope stability analysis.'' *Symp. on Unsaturated Soil Behavior and Applications*, Nairobi, Kenya, 1–31.
Rinaldi, V. A., Santamarina, J. C., and Redolfi, E. R. (1998). ''Characterization of collapsible soils with combined geophysical and penetration testing.'' *Proc., 1st Int. Conf. on Site Characterization, ISC'98*, P. K. Robertson and P. W. Mayne, eds., Balkema, Brookfield, 581–588.
Sahimi, M. (1994). *Applications of percolation theory*, Taylor and Francis, London.
Santamarina, J. C., and Aloufi, M. (1999). ''Small strain stiffness: A micromechanical experimental study.'' *Proc. of Pre-failure Defor. Char. of Geomaterials, IST99*, M. Jamiolkowski, R. Lancellotta, and D. Lo Presti, eds., Balkema, The Netherlands, 451–458.
Santamarina, J. C., and Cascante, G. (1996). ''Stress anisotropy and wave propagation—A micromechanical view.'' *Can. Geotech. J.*, Ottawa, 33, 770–782.
Santamarina, J. C., and Wakim, Y. N. (1992). ''Principles of ground modification with electromagnetic waves: Applications to environmental geotechnology.'' *Grout., Soil Impr. and Geosyn.*, ASCE-SP, (Feb.), 1380–1392.
Skempton, A. W. (1961). ''Horizontal stresses in an over-consolidated Eocene clay.'' *Proc., 5th Int. Conf. for Soil Mech. and Found. Engrg.*, Dunod, Paris, 351–357.
Stokoe, K. H., II, Lee, J. N.-K., and Lee, S. H.-H. (1991). ''Characterization of soil in calibration chambers with seismic waves.'' *Proc., 1st Int. Symp. on Calibration Chamber Testing*, 363–376.
Terzaghi, K. V. (1925). ''Principles of soil mechanics: I—Phenomena of cohesion of clay.'' *Engrg. News Record*, 95(19), 742–746.
Terzaghi, K. V., and Peck, R. B. (1948). *Soil mechanics and engineering practice*, Wiley, New York.
Trevena, D. H. (1987). *Cavitation and tension in liquids*, Hilger, London.
Wu, S., Gray, D. H., and Richart, F. E., Jr. (1984). ''Capillary effects on dynamic modulus of sands and silts.'' *J. Geotech. Engrg.*, ASCE, 110(9), 1188–1203.